Nuclear Physics A548 (1992) 453–470
North-Holland

NUCLEAR
PHYSICS A

Cross sections and mean angular momenta for $^{64}Ni + ^{92,96}Zr$ fusion near and below the Coulomb barrier

A.M. Stefanini, L. Corradi, D. Ackermann, A. Facco, F. Gramegna, H. Moreno[1], L. Mueller, D.R. Napoli, G.F. Prete and P. Spolaore

Istituto Nazionale di Fisica Nucleare, Laboratori Nazionali di Legnaro, I-35020 Legnaro, Padua, Italy

S. Beghini, D. Fabris, G. Montagnoli, G. Nebbia, J.A. Ruiz[2], G.F. Segato, C. Signorini and G. Viesti

Dipartimento di Fisica, Università di Padova, and Istituto Nazionale di Fisica Nucleare, Sezione di Padova, I-35100, Padua Italy

Received 15 April 1992

Abstract: Fusion cross sections and mean angular momenta have been measured for $^{64}Ni + ^{92,96}Zr$ around the Coulomb barrier. The results are presented and systematically compared with the predictions of a schematic coupled-channel model, demonstrating the need of more refined calculations including higher-order coupling effects, and/or other degrees of freedom, beyond the usual inelastic and quasi-elastic transfer channels.

E

NUCLEAR REACTIONS $^{92,96}Zr(^{64}Ni, X)$, $E = 202$–269 MeV, measured evaporation residues, $\gamma\gamma$-coin; deduced fusion $\sigma(E)$, average spin distribution around, below Coulomb barrier. Coupled-channel calculations. Enriched targets, recoil mass spectrometer, electrostatic beam separator.

1. Introduction

It is qualitatively established that the very large heavy-ion fusion cross sections observed below the Coulomb barrier are a manifestation of channel coupling effects. Inelastic scattering to low-lying states (surface vibrations) and quasi-elastic nucleon transfer between the colliding nuclei have usually been considered by the models for coupled-channel (CC) calculations of fusion; refs. [1,2]) give broad overviews of this field. Theories are able to reproduce the experimental data for light and/or very asymmetric systems to a satisfactory degree of accuracy. On the other hand, the data for heavier and nearly symmetric systems cannot be reproduced by standard CC calculations.

Similar evidences come from the studies of spin distributions, or mean angular momenta leading to fusion in the vicinity of the barrier. It has been shown [3]) that where both $\langle l \rangle$ values (through γ-multiplicity) and fusion cross sections are available,

[1] On leave from University of Sevilla, Spain.
[2] On leave from University of Valencia, Spain.

the CC model underpredicts both quantities at barrier energies and below for heavy (quasi-)symmetric systems, whereas it works rather well for light and/or asymmetric ones.

Here we report on the measurements of fusion excitation functions and $\langle l \rangle$ values for $^{64}Ni + ^{92,96}Zr$ in an energy range encompassing the barrier. The purpose of these experimental investigations was twofold: (1) to extend the very limited systematics existing for such rather heavy systems, comparing at the same time the experimental results with the CC model, and (2) to check a striking difference [4]) between the spin distributions around the barrier in the two cases, the one for ^{96}Zr being broader and clearly below the unitarity limit even at low angular momenta.

A previous measurement of evaporation residue (ER) cross sections exists for $^{64}Ni + ^{92}Zr$ [ref. [5])]; ER cross sections and $\langle l \rangle$ values at three energies around the barrier [6]) are also available for $^{64}Ni + ^{96}Zr$, including measurements of complete spin distributions for both systems [see ref. [4]) and references therein], but only at one energy. A preliminary report of the present experiments has already been published [7]), it was limited to the ER excitation functions. This paper is a more complete presentation of those results, as well as of the more recent experiments on $\langle l \rangle$ values in the same energy range.

In sect. 2 the set-ups are described and the raw experimental data (cross sections and γ-ray multiplicities) are presented. Sect. 3 contains a detailed analysis of the procedure used to extract the mean angular momenta. In sect. 4 fusion excitation functions and $\langle l \rangle$ values are compared with the results of CC calculations. Sect. 5 is a summary of this work and an outlook at future experimental and theoretical developments.

2. Experimental

The experiments were performed at the XTU Tandem accelerator facility of the Laboratori Nazionali di Legnaro, using ^{64}Ni beams in the energy range 202–269 MeV. Typical beam currents were 0.5–1.5 pnA. The targets for the ER excitation function measurements were metallic $^{92,96}Zr$ evaporated on 20 $\mu g/cm^2$ carbon layers, with thicknesses 165 and 50 $\mu g/cm^2$ and isotopic enrichments 94.57% and 95.63%, respectively. For the $\langle l \rangle$ measurements we used $^{92,96}ZrO_2$ strip evaporations ($\simeq$1 mm wide) on similar carbon backings; the thicknesses were 200 $\mu g/cm^2$ for both targets, enriched to 98.06% and 95.63% in mass 92 and 96, respectively.

The set-up for the ER cross section measurements has been described in detail elsewhere [8]). It is built up from an electrostatic beam deflector followed by a time-of-flight energy telescope with a micro-channel plate detector and a silicon surface barrier detector. ER yields at 0° and at small angles were measured. Two silicon detectors were placed at $\theta_{lab} = 17.5°$ for normalization purposes. Complete ER angular distributions were obtained at $E_{lab} = 225.5$, 237.0 and 262.0 MeV as shown in fig. 1. At the two lower energies the widths and shapes of those distributions

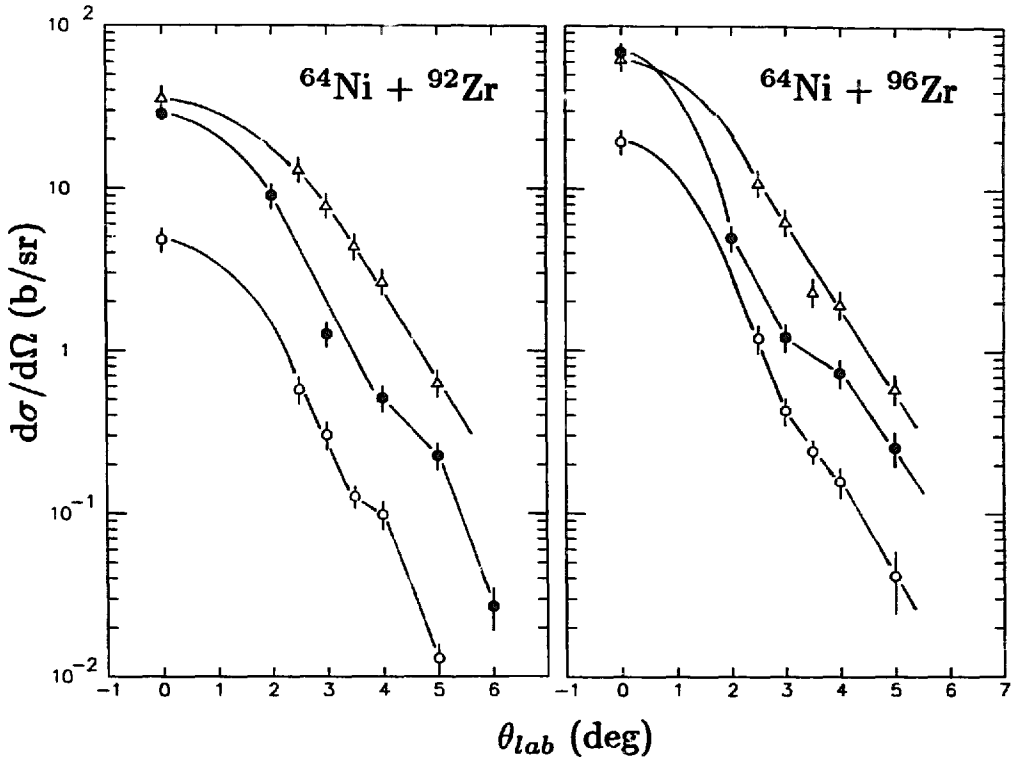

Fig. 1. Angular distribution of evaporation residues from the indicated reactions. The ^{64}Ni beam energies were 225.5 MeV (open circles), 237.0 MeV (full circles) and 262.0 MeV (triangles). The lines through the experimental points are only to guide the eye.

do not vary significantly for both targets, but at 262 MeV a certain broadening shows up, due to contributions from charged particle evaporation channels. Neutron evaporation is in any case much more likely for $^{64}Ni + ^{96}Zr$ [see the measurements of ref. [6])], and this is reflected in more forward-peaked ER angular distributions. The integral ER cross sections were obtained via inter- and extrapolations of those distributions for the energies where the yields were measured at 0° only. Further corrections were applied for the target isotopic compositions. The final results are listed in the second column of tables 1 and 2, where the quoted energies are corrected for the target thicknesses.

The experimental errors include uncertainties due to the angular distribution integrations, to the determination of the monitors position and transmission of the electrostatic deflector and their respective solid angles [see ref. [8])], and finally to the statistical part. The overall contribution of the systematic errors is estimated around ±17%. The measured ER cross sections are shown in fig. 2, together with the results of calculations which will be discussed later.

Two different experimental arrangements have been used for the measurement of average angular momenta connected with fusion evaporation for the two systems. In the case of the ^{96}Zr experiment the recoil mass spectrometer (RMS) [10]) was used. It was operated at 0° and at small angles in coincidence with an array of four 4″ × 4″

TABLE 1

Experimental ER cross sections [see also ref. [7]], mean γ-ray multiplicities and deduced average angular momenta, for the system $^{64}Ni + ^{96}Zr$

$E_{c.m.}$ (MeV)	σ_{ER} (mb)	$\langle M_\gamma \rangle$	$\langle l \rangle$ ($\hbar$)
120.6		4.0 ± 1.4	9.3 ± 3.3
121.6	0.26 ± 0.04	5.9 ± 1.0	13.0 ± 1.8
124.0	2.44 ± 0.31	8.6 ± 1.2	17.0 ± 3.3
126.4	8.31 ± 1.52	9.7 ± 1.4	19.3 ± 2.6
128.8	19.3 ± 3.5	11.2 ± 1.3	22.2 ± 2.9
131.4	44.3 ± 8.1	12.2 ± 1.5	23.3 ± 3.1
134.4	83.2 ± 14.8	14.0 ± 1.3	27.4 ± 2.6
136.8	122.1 ± 21.3	14.8 ± 1.8	27.0 ± 3.4
139.5	166.1 ± 29.2		
141.3	176.2 ± 30.5	16.[illegible] ± 1.5	30.8 ± 2.8
144.5	185.7 ± 32.0		
147.9	187.1 ± 32.0	19.7 ± 1.9	38.9 ± 3.5
152.1	215.2 ± 36.8		
156.3	250.3 ± 44.2	21.1 ± 1.6	44.1 ± 2.9
160.5	270.6 ± 47.5		

NaI(Tl) crystals placed at ~20 cm from the target, at 55° or at 125° with respect to the beam direction; each of them was inserted in a cylindrical lead shield, 4 cm thick. The NaI crystals detected the prompt γ-rays in the energy range ≃100 keV–3 MeV. The RMS rejects effectively the beam and beam-like particles, while dispersing at the same time the ions of interest along the focal plane according to the A/q ratio (mass over ion charge state). The focal plane detector is a 12×7 cm^2 multi-wire proportional counter (MWPC), giving X, Y and time signals, X being the ion

TABLE 2

Same as table 1, but for $^{64}Ni + ^{92}Zr$

$E_{c.m.}$ (MeV)	σ_{ER} (mb)	$\langle M_\gamma \rangle$	$\langle l \rangle$ ($\hbar$)
122.2	0.028 ± 0.014		
124.5	0.222 ± 0.043		
125.6		5.5 ± 1.2	16.9 ± 2.1
126.8	1.24 ± 0.24	6.6 ± 1.9	18.8 ± 3.1
129.4	5.58 ± 1.0	8.0 ± 1.1	20.1 ± 1.8
132.3	20.9 ± 3.7	9.3 ± 1.1	21.4 ± 1.8
134.6	41.2 ± 7.2	10.0 ± 1.2	21.7 ± 2.0
137.2	74.0 ± 12.9	10.9 ± 1.4	22.6 ± 2.3
138.9	100.5 ± 17.2	10.8 ± 1.2	23.6 ± 1.9
142.0	136.4 ± 23.3		
145.4	165.7 ± 28.3	13.6 ± 1.8	35.5 ± 2.9
149.5	214.1 ± 36.5		
153.6	226.0 ± 39.0	12.2 ± 1.2	38.1 ± 1.9
157.8	248.3 ± 42.8	11.9 ± 1.2	39.8 ± 1.9

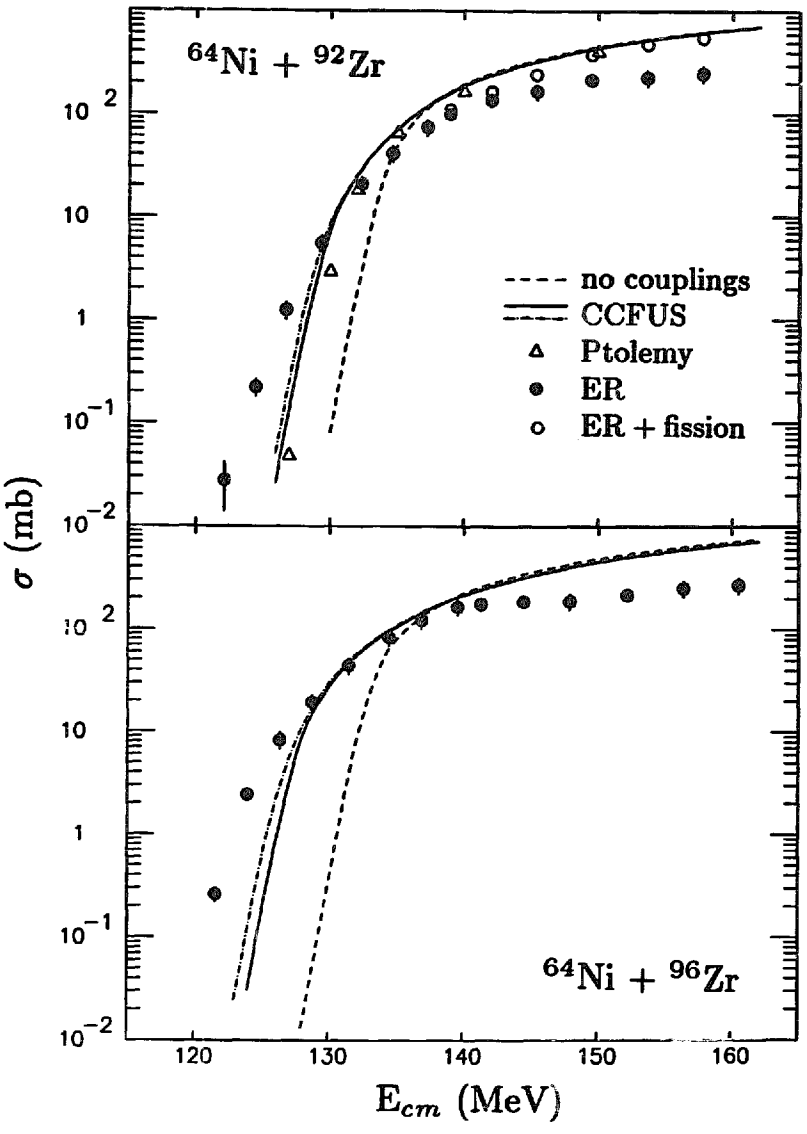

Fig. 2. Evaporation residue excitation functions. In the case of $^{64}Ni + ^{92}Zr$ only, compound nucleus fission yields[9]) have been added to the present ER data. The lines are the results of coupled-channel calculations (see text), including the lowest 2^+ and 3^- excitations (full lines), and in addition two transfer channels (dash-dotted lines).

position along the dispersion plane. The MWPC is followed by an ionization chamber with axial electric field, giving the total energy E and the Bragg-peak height BP of the ion. The beams were pulsed (3-4 ns FWHM, one pulse every 800 ns) and the time of flight t.o.f. of the ions through the spectrometer was also recorded.

The residual beam-like background was most conveniently separated from the ER in the two-dimensional plots t.o.f. versus E and/or t.o.f. versus X. Sometimes the matrix BP versus E was used too. Fig. 3 (upper panel) shows a 0° scatter plot t.o.f. versus $X \simeq A/q$, where one can see three groups of evaporation residues corresponding to the indicated charge states; within each group three masses can

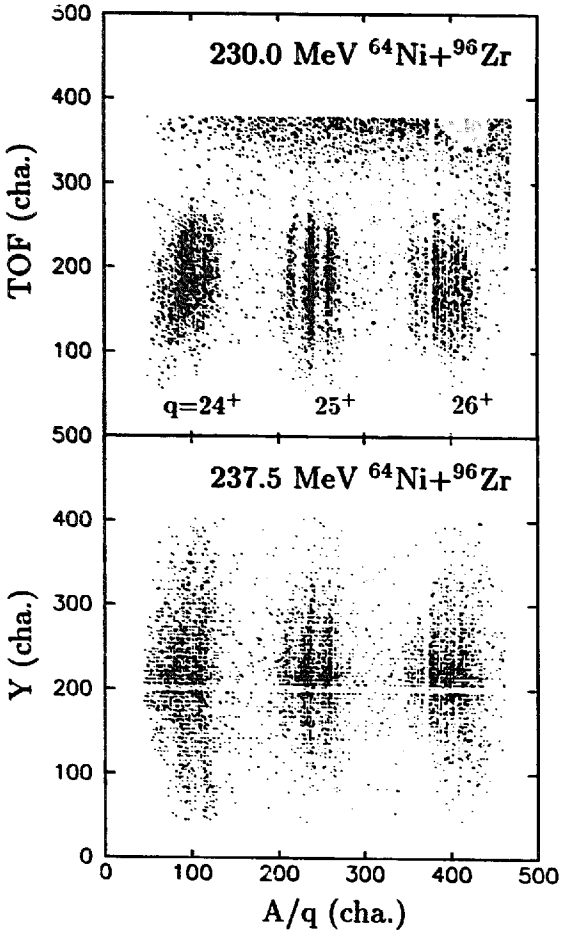

Fig. 3. Scatter plots of t.o.f. versus $X = A/q$, and Y versus A/q for $^{64}Ni+^{96}Zr$ at the two indicated energies, recorded at 0°. Within each charge state group, the three masses are $A = 158$, 157 and 156 (increasing towards the left side).

be seen. The events in the upper part of the panel are residual beam-like particles (which have different t.o.f.). By selecting the ER groups we have obtained clean X, Y scatter plots, as shown in the lower panel for another energy. The mass resolution was better in the center of the focal plane, and the 'hole' in the middle of the Y-coordinate is due to a missing wire of the MWPC.

Fig. 4 shows two mass spectra recorded for ^{96}Zr, after proper ER selection, at a rather low energy, ~7% below the nominal barrier, where the fusion cross section is around 8 mb. The three groups in each spectrum correspond to the ion charge states 24^+, 25^+ and 26^+. The dominant evaporation channels are 3n and 2n; the yield of the latter is enhanced if coincidence with γ-rays is required (lower panel), due to the higher spin, i.e. γ-multiplicity associated with fewer neutrons emission.

The mean γ-multiplicities associated with each residual mass were deduced from

$$\langle M_\gamma \rangle = \frac{N_c}{N_s} \frac{1}{\langle \varepsilon_\gamma \rangle} - M_n \frac{\langle \varepsilon_n \rangle}{\langle \varepsilon_\gamma \rangle}, \tag{1}$$

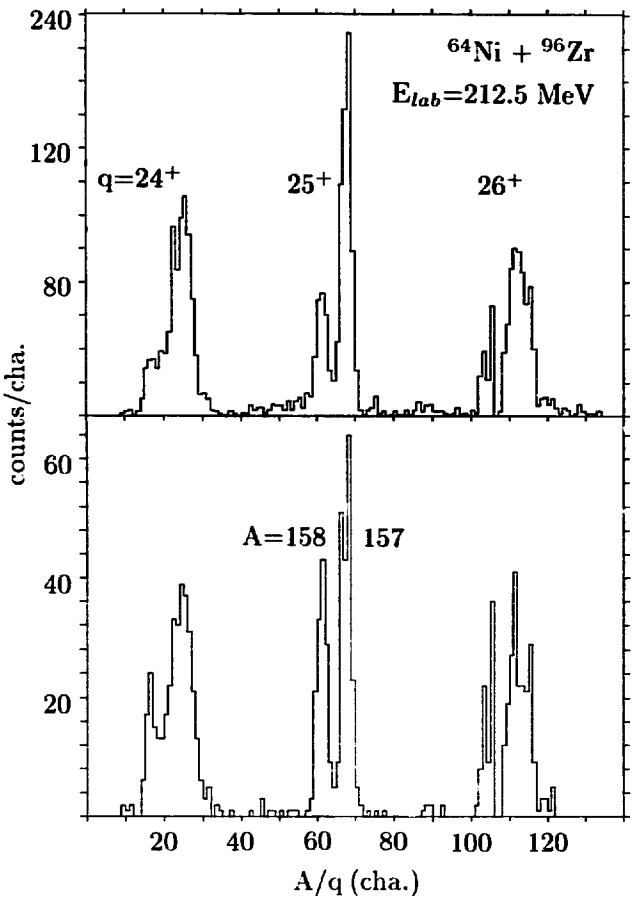

Fig. 4. Mass spectra of ER from the indicated reaction obtained from the recoil mass spectrometer (upper panel). The three groups correspond to the ion charge states 24^+, 25^+ and 26^+. The spectrum in the lower panel was measured when we required a coincidence with at least one prompt γ-ray.

where N_c (N_s) is the number of counts in a particular mass peak with a (without any) coincidence requirement with any γ-ray. $\langle\varepsilon_\gamma\rangle$ is the combined absolute efficiency of the NaI array, averaged over the selected energy range. It was measured by placing ^{60}Co and ^{152}Eu γ-sources at the target position. $\langle\varepsilon_n\rangle$ is the efficiency of the array for detecting neutrons and M_n is the corresponding neutron multiplicity. This procedure is analogous to that of Gil *et al.* [11]), and we took $\langle\varepsilon_n\rangle/\langle\varepsilon_\gamma\rangle = 0.12$ for our larger detectors [see also ref. [12])]. The corrections for the cross-talk between the γ-detectors and for the probability of double-hitting events were found to be very small, according to off-line tests with the γ-sources. They were, therefore, neglected in the analysis. We state that this method for extracting mean γ-multiplicities is independent of the RMS transmission.

For the $\langle I\rangle$ measurements in $^{64}Ni + ^{92}Zr$ we exploited two set-ups. At three ^{64}Ni energies (216, 248.5 and 262.5 MeV) the RMS in coincidence with the array of NaI detectors was used, whereas for the complete $\langle I\rangle$ excitation function, including those three energies, the electrostatic deflector+t.o.f.-E telescope (where we measured

the ER cross sections, see above) was operated in coincidence with two of the NaI detectors, placed at 90° to the beam line and at ~10 cm from the target. Hence, apart from the different geometry of the arrangement, the method for deducing $\langle M_\gamma \rangle$ follows strictly the one described above, although the t.o.f.-E telescope has only a limited mass resolution, quite insufficient to distinguish between two near-by masses in the region of interest ($A \simeq 150$). Therefore, we derived $\langle M_\gamma \rangle$ for the whole group of ER, and the three measurements with the RMS were used to obtain high-resolution ER mass spectra at representative energies, which, together with the data already available from the literature around the barrier [13,14]), yielded us the evaporated particles multiltiplicities. This information was interpolated in the whole studied energy range and is essential in the conversion of γ-multiplicities to spin. Consistency checks were also performed with the second set-up for $^{64}Ni + ^{96}Zr$ at selected energies, and the resulting γ-multiplicites are in good agreement with the data from the RMS, when we average the multiplicities of the various evaporation channels, weighting them with the corresponding relative cross sections.

The reason for using the electrostatic deflector was the known existence of various isomers in most of the evaporation channels from $^{64}Ni + ^{92}Zr$ fusion. The half-lives are in the range of ~30 to 400 ns, so that their decay happens in-flight inside the RMS (transit times were 600–700 ns). Such events are lost from the mass spectra at the focal plane if the ion charge state changes as a consequence of internal conversion followed by an Auger cascade. This is not the case when using the electrostatic deflector, where (1) the ER flight times were around 200 ns, so that the longer-lived isomers mostly decay inside the stop detector, and (2) the collection efficiency is constant over many ion charge states (due to the detector geometry and to the small deflection angle [8]); hence, even nuclei with shorter-lived isomers, those in the 30 ns half-life range, are effectively collected with this set-up. The subsequent (non-trivial) problem of how to take into account the isomer population in the data reduction will be analyzed in the following section.

A correction has to be applied to the raw γ-multiplicities, for their dependence on the ER detection angle. This becomes important when charged particle evaporation channels are not negligible (α-particles in particular), as those channels have in general less forward-peaked angular distribution and lead to ER with lower angular momenta with respect to the pure neutron evaporation cases. Qualitatively it is expected that lower γ-multiplicities are associated with ER detected out of 0°. In the case of $^{64}Ni + ^{92}Zr$ measurements at 3° and 5° were performed at 237.5 and 262.5 MeV. In both cases a regular decrease of the multiplicities has been observed (~30% when going from 0° to 5°). Therefore, weighted averages of the multiplicities have been derived, considering the ER cross sections at the different angles (see fig. 1), and the results have been interpolated and extrapolated for the other energies. There is no analogous correction for $^{64}Ni + ^{96}Zr$, as neutron evaporation is dominant in this case and as the RMS acceptance angle was anyway rather wide around 0° (±3°, corresponding to a geometric solid angle of 5 msr).

TABLE 3

Measured mean γ-ray multiplicities and deduced average angular momenta, for individual neutron evaporation channels from $^{64}Ni+^{96}Zr$. $\langle I\rangle$ values are in units of $\hbar$.

$E_{c.m.}$ (MeV)	$M_\gamma(2n)$	$M_\gamma(3n)$	$M_\gamma(4n)$	$M_\gamma(5n)$	$\langle I\rangle(2n)$	$\langle I\rangle(3n)$	$\langle I\rangle(4n)$	$\langle I\rangle(5n)$
124.0	13.9±2.9	5.8±1.2			23.6±5.4	13.5±2.2		
126.4	15.0±2.4	7.9±1.0	4.5±2.9		25.8±4.5	17.3±1.8	7.1±5.4	
128.8	16.9±2.9	9.8±1.1	9.2±3.5		29.2±5.4	20.9±2.0	15.7±6.5	
131.4	19.3±3.4	11.2±1.2	8.8±2.1		33.0±6.3	22.7±2.2	14.3±4.0	
134.4	22.7±3.0	14.6±1.1	11.7±1.4		38.5±5.7	28.4±2.1	18.8±2.6	
136.8	23.8±4.4	14.7±1.5	11.4±1.7		40.6±8.3	28.6±2.8	18.5±3.2	
141.3	23.3±3.4	16.6±1.3	14.2±1.3		40.0±6.3	33.2±2.5	25.1±2.4	
147.9		22.8±2.3	19.9±1.6	11.0±1.9		45.4±4.3	36.7±3.0	27.8±3.6
156.3		25.5±2.5	23.4±1.5	14.4±1.2		51.1±4.6	44.9±2.8	35.1±2.2

Finally, one should take into account the γ-ray angular distributions which were measured for both systems [15]) around the barrier. The results show a slight asymmetry for the ^{92}Zr target and a more pronounced one for ^{96}Zr, essentially due to the predominance of E2 collective transitions in this latter case. In our experiment with ^{96}Zr, the NaI crystals were placed at 55°, where the angular distribution effects are cancelled, while with ^{92}Zr the detectors were at 90° but a large angle ($\pm\simeq 20°$) was covered, so that the angular distribution effects may safely be neglected. Tables 1 and 2 list the final $\langle M_\gamma\rangle$ values in the third column. The quoted errors are the statistical uncertainties plus a contribution of the order of ±5% from the determination of the mean γ-ray efficiencies. Table 3 reports the mean multiplicities for the individual evaporation channels from $^{64}Ni+^{96}Zr$, apart from the two lowest measured energies where the statistics did not allow such a detailed analysis.

3. $\langle M_\gamma\rangle$ to $\langle I\rangle$ conversion

In early experiments [see e.g. refs. [6,16,17])] the conversion from γ-multiplicities to angular momenta has often been accomplished by using simple relationships of the type $\langle I\rangle = a(\langle M_\gamma\rangle - b) + c$, where a is meant as the spin removed per non-statistical γ-ray, b is the number of statistical dipole transitions which carry away very little angular momentum, and c is a correction for the ground-state spin of the residual nuclei. It has been shown by more recent analyses [11,18–20]) that the resulting $\langle I\rangle$ values are questionable, especially below 8–10$\hbar$ where there is a substantial loss of sensitivity of γ-multiplicity to spin, and that the angular momentum removed by evaporated particles has to be explicitly included in the conversion. Moreover, a detailed knowledge of ground-state spins and/or long-lived isomers of the ER is necessary.

This is the reason why we follow the line indicated by such recent studies to convert multiplicities into spin. We point out, anyway, that the final $\langle I\rangle$ values which

we obtained are only marginally different (considering the experimental errors) from what we have calculated from the simple relationship presented above. In the energy region around the barrier ($\langle l \rangle \simeq 20$–$25\hbar$) the disagreement with theory is quite large, as we shall see in the following, whatever (reasonable) procedure is used to derive angular momenta from multiplicities. We adopted, at each energy, the transformation

$$\langle l \rangle = \Delta I_{n_s}(\langle M_\gamma \rangle - M_{\gamma_s}) + \Delta I_s M_{\gamma_s} + \Delta I_{n,p} M_{n,p} + \Delta I_\alpha M_\alpha + \Delta I_{ec} + \langle I_0 \rangle , \qquad (2)$$

where ΔI_{n_s} is the spin removed per non-statistical photon, M_{γ_s} is the multiplicity of statistical dipole transitions, ΔI_s is the spin removed by such statistical γ-rays, $M_{n,p}$ and M_α are the numbers of evaporated neutrons and/or protons, and α-particles, respectively, $\Delta I_{n,p}$ and ΔI_α are the corresponding average amounts of angular momentum carried off, $\Delta I_{ec} \simeq 1$ is a small correction [18]) for internal conversion events, and $\langle I_0 \rangle$ is the average of the ground-state spin and of the isomeric level spin in the residual nucleus, weighted over the relative population probability.

The only important isomer in the ER following $^{64}Ni + ^{96}Zr$ fusion is the 76ms $\frac{9}{2}^+$ level in ^{157}Er. In analogy with ref. [18]), we have assumed that 90% of the flux into that nucleus feeds the isomer at all energies (it is yrast and only 155 keV above the ground state). In the case of $^{64}Ni + ^{92}Zr$ high-spin isomers are present in all evaporation channels, and spins and excitation energies are known in most cases. We performed a detailed analysis of the γ-spectroscopic data available [21]), such as level schemes, γ-ray intensities and branching ratios, and isomer population probabilities with heavy-ion reactions. Independently, we have relied on the $\langle l \rangle$ values extracted for the corresponding evaporation channels of $^{64}Ni + ^{96}Zr$ (this work) and $^{64}Ni + ^{100}M$ [ref. [19])], where practically no isomers are present, to assess to which extent the deexcitation flux in a particular nucleus may be trapped in the isomeric level. All this gave us, with some additional extrapolations, the isomers population probability at each energy. The procedure is by no means free from uncertainties, as γ-ray spectroscopic data are not as complete as one would need, and as only an additional detailed knowledge of the spin distributions would solve the puzzle; but measuring the spin distributions, or at least $\langle l \rangle$ values, is just the aim of the present experimental work.

M_{γ_s}, $\Delta I_{n,p}$ and ΔI_α were calculated with the code PACE2 [22]), using default parameters. Typical values for M_{γ_s} are 1.5–3, depending on the energy, and similarly we get $\Delta I_{n,p} = 0.5$–1.3 and $\Delta I_\alpha = 2.0$–10.0. ΔI_s was fixed to 0.3 independent of the energy [18]), and ΔI_{n_s} has been taken 1.87 for $^{64}Ni + ^{96}Zr$ based on the same work [18]) on $^{34}S + ^{130}Te$; for $^{64}Ni + ^{92}Zr$ it has been fixed to 1.65 following the work of Ruckelshausen *et al.* [23]) on this system. The difference between the two numbers qualitatively reflects the larger relative amount of stretched E2 collective transitions in the ER from the more neutron-rich ^{160}Er compound nucleus.

The way we chose $M_{n,p}$ and M_α is different for the two systems: for $^{64}Ni + ^{96}Zr$ mean angular momenta were deduced for the individual evaporation channels from

the corresponding $\langle M_\gamma \rangle$ values. In this system charged particle evaporation is very small [6]) around the barrier, and this can safely be extrapolated to subbarrier energies. As we could only distinguish between different masses, we cannot experimentally assess the possible increasing importance of (p, xn) channels above the barrier. Protons and neutrons are anyway expected to remove comparable quantities of angular momentum. As for the (α, xn) channels, they were not observed in the RMS spectra over the background level ($\simeq$1-2%) at all energies. According to the statistical model calculations, there are non-negligible contributions at the two highest measured energies, with α multiplicities not exceeding $\simeq$0.1. This leads to small corrections ($\leq$1-1.5$\hbar$) which were applied after averaging the $\langle l \rangle$ values of the various neutron (and/or proton) evaporation channels.

In the case of $^{64}Ni + ^{92}Zr$ we had ER mass spectra from the RMS at three energies only, whereas the bulk of the measurements with the electrostatic deflector gave only total ER yields. On the basis of previous work at barrier energies [13,14]), and interpolating those three high-resolution mass spectra, we deduced *mean* particle

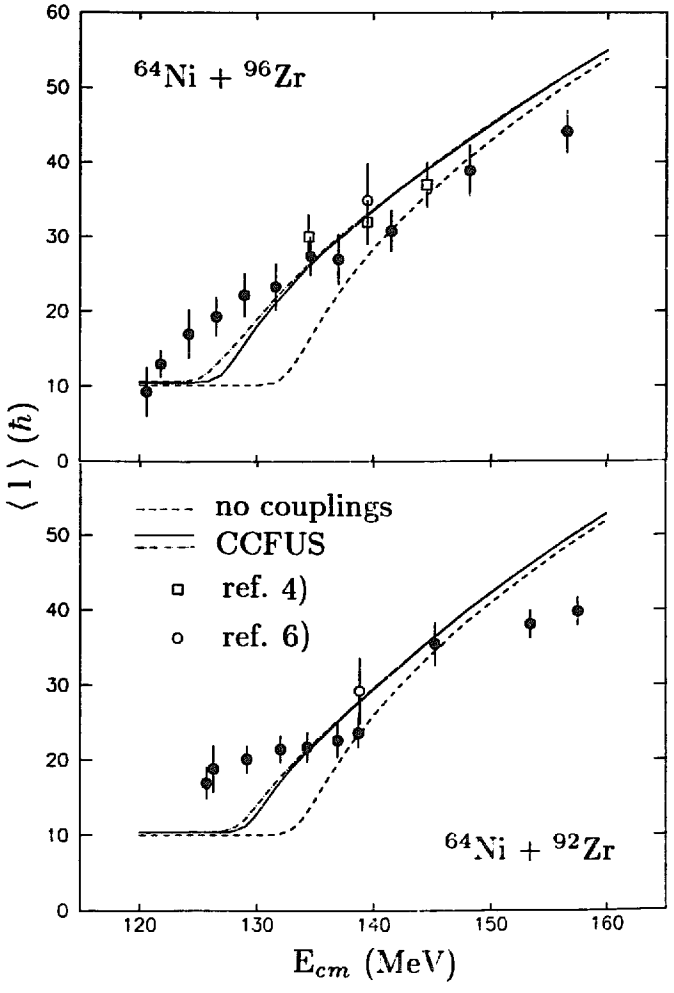

Fig. 5. Mean angular momenta leading to fusion evaporation versus energy. The present results are the full circles. See the caption of fig. 2 for the explanation of the lines.

multiplicities to be inserted in eq. (2) at all energies. Hence, we obtained $\langle l \rangle$ values directly averaged over the evaporation channels. We point out that in $^{64}Ni+^{92}Zr$ (α, xn) channels, being 12–14% of the total ER cross section already at the barrier, have a larger influence on the spin, but their contribution does not exceed 2–3$\hbar$ even at the highest energies.

The final $\langle l \rangle$ values are listed in tables 1 and 2 (column 4); table 3 contains the $\langle M_\gamma \rangle$ and $\langle l \rangle$ values for each neutron evaporation channel from $^{64}Ni+^{96}Zr$ fusion. The values of the γ-multiplicities reported in table 3 at 134.4 MeV are in excellent agreement with the results published in ref. [6]) for the same energy. We do not comment any more on the data of table 3, as the aim of this work is not to investigate the compound nucleus decay, but rather how it is formed.

The quoted errors in the tables are simply derived from the uncertainties adopted for the γ-multiplicites (see above). We are aware that the actual errors on the $\langle l \rangle$ values are surely larger, as the procedure for transforming multiplicities into angular momenta contains avoidable assumptions and approximations. But it is quite difficult to estimate quantitatively the corresponding uncertainties. For example, the population of isomers and the results of statistical model calculations depend to some extent on the quantity which is the goal of the experiments, i.e. the compound nucleus spin distribution. This is also the reason why we decided to not vary the parameters of such calculations, based on the substantial agreement of the results with that obtained from simpler transformations, as stated above; good agreement is also found with previous measurements for the same systems [4,6]), where the experimental arrangements were different as well as the assumptions and parameters used in the analysis of γ-multiplicity data.

Fig. 5 shows the data listed in tables 1 and 2, as a function of the energy. The lines correspond to various coupled-channel calculations discussed below.

4. Discussion

The fusion excitation functions for $^{64}Ni+^{92,96}Zr$ are shown in fig. 2. Compound nucleus fission cross sections have been measured for the ^{92}Zr target only [9]), so that they have been added to the ER data in the plot. The experimental results are compared with the predictions of simplified coupled-channel (CC) calculations performed with a modified version of the code CCFUS [24]), where the lowest quadrupole and octupole inelastic excitations of both projectile and target have been independently coupled to the entrance channel (full lines). The coupling strengths have been derived from the experimental $B(E\lambda)$ values [25]) for those excitations. The ion–ion potential used is an empirical Woods–Saxon parametrization [26]) of the Christensen–Winther potential [27]), which fits its tail, and it reads

$$U(r) = -31.67 \frac{R_1 R_2}{R_1 + R_2} \frac{1}{1 + \exp\left[(r - R_1 - R_2 - \Delta R)/a\right]} \text{ MeV}, \qquad (3)$$

where $R_i = 1.233 A_i^{1/3} - 0.98 A_i^{-1/3}$ fm, $a = 0.63$ fm and ΔR has been fixed to 0.0 fm in the present case. No attempt to vary such parameters was made.

Large underpredictions of the experimental cross sections show up at sub-barrier energies for both systems, while a satisfactory agreement is found at higher energies for $^{64}Ni+^{92}Zr$. Such a comparison is not possible for $^{64}Ni+^{96}Zr$, where the ER yields flatten out above the barrier, as expected due to fission competition. In order to check the CC results, we performed also exact CC calculations with the code PTOLEMY [28]) at selected energies for $^{64}Ni+^{92}Zr$, with the same ion-ion potential and a sharp absorptive term confined inside the barrier, to simulate an ingoing-wave boundary condition. This may be regarded as too crude an assumption, also in view of recent theoretical analyses [29]), but we feel it reasonably appropriate when checking for large and systematic effects as it is in this work. The PTOLEMY results are reported in fig. 2 as triangles and it appears that the large discrepancies at low energies cannot be attributed to the approximations inherent to CCFUS.

The situation is similar in the near-by system $^{64}Ni+^{100}Mo$ [ref. [19])]. In that case, a different Woods-Saxon potential was employed in the CC analysis, but we checked that the use of the empirical potential described above gives results practically coincident with the calculations reported in that work around and above the barrier and only increases by not more than a factor two in the sub-barrier cross sections. A very large underprediction of the low-energy fusion data is observed anyway.

One might argue that coupling even quasi-elastic transfer channels would fill the gap between theory and experiment, in our cases as well as in $^{64}Ni+^{100}Mo$. Preliminary results have been reported [30]) for the measurement of transfer in $^{64}Ni+^{100}Mo$, indicating very small cross sections. As for our systems, no experimental data are yet available on transfer. We decided to perform model calculations with CCFUS, where, in addition to the inelastic excitations, we introduced two transfer channels with coupling strengths arbitrarily fixed to 1 MeV and Q-values corresponding to those for one- and two-neutron pick-up between ground states. We see from fig. 2 (dash-dotted lines) that the effect is slightly larger in the case of $^{64}Ni+^{96}Zr$, where $Q_{g.s.}(2n)$ is positive (+0.93 MeV), but in general such transfer channels are predicted to only slightly reduce the data underestimation.

We mentioned in the Introduction that one of our purposes was to check a large isotopic difference [4]) between the two systems at near-barrier energies, i.e. the spin distribution of $^{64}Ni+^{92}Zr$ was found to exhaust the unitarity limit for low angular momenta, while fusion of $^{64}Ni+^{96}Zr$ evidenced a broader distribution with cross sections which do not reach the unitarity limit even for small partial waves. Now, the absolute partial wave cross sections in ref. [4]) relied on previous determinations of the integral ER cross sections. As already stressed in our previous work [7]), where a fuller discussion of this point can be found, the present ER cross sections agree well with the older data [6]) for $^{64}Ni+^{96}Zr$, while serious discrepancies show up for $^{64}Ni+^{92}Zr$. As a matter of fact, we get $\sigma_{ER} \simeq 100$ mb at $E_{c.m.} = 138.9$ MeV where the complete spin distribution was measured [4]), whereas the older result [5]) is a factor $\sim$2.4 larger. Consequently, the present data indicate that there is no striking isotopic effect in the spin distribution: in both systems the unitarity limit is not reached even for small partial waves. The only difference is the somewhat broader spin distribution

of $^{64}Ni + ^{96}Zr$, which needs to be understood on the basis of the CC theory.

The results of $\langle l \rangle$ measurements are summarized in fig. 5 together with the previously available data, and the agreement is generally good. At high energy the compound nucleus fission sets in and, correspondingly, the ER $\langle l \rangle$ values begin to saturate and to fall below the theoretical predictions for fusion. This is seen in both systems, showing that fission becomes rapidly the dominant decay mode above the barrier in both cases, although it has not been measured for $^{64}Ni + ^{96}Zr$, in agreement with what we deduce from the ER excitation functions. In a preliminary report of the present data [31]), a different behaviour of the two systems seemed apparent at high energies; we have realized, however, that it was only due to some unfortunate mishandling of the raw data.

The lines in fig. 5 are the predictions of the same calculations discussed above in connection with the integral fusion cross sections. In both systems $\langle l \rangle$ exceeds by a factor up to ~ 2 the CC results in the energy range around the barrier where coupling effects show up most strongly, thereby connecting the high-energy classical sharp (or smooth) cut-off regime with the low-energy quantal regime where constant $\langle l \rangle$ are predicted [32,33]). Here again the calculated effect of the neutron transfer channels is small.

A similar behaviour is shown by $^{64}Ni + ^{100}Mo$, where $\langle l \rangle$ (as well as complete partial-wave distributions) were measured at Oak Ridge [19]), and, as already evidenced for fusion cross sections, the CC calculations are well below the data for $\langle l \rangle$ too.

We may conclude that for these heavy and nearly symmetric systems both fusion cross sections below the barrier and mean angular momenta around the barrier are not satisfactorily reproduced by standard CC calculations. Such twofold failure of the model is pictorially shown in fig. 6, where the ER cross sections are plotted versus the corresponding average spins. The σ versus $\langle l \rangle$ relation is predicted to be practically identical for the two systems in the no-coupling limit (dashed line), while, of course, differences show up in the CC calculations including the 2^+ and 3^- inelastic excitations (full line for $^{64}Ni + ^{92}Zr$ and dashed-dotted line for $^{64}Ni + ^{96}Zr$). In such a presentation the energy does not appear, and the experimental points for the two systems show a tendency to approach the predicted constant angular momentum at small cross sections. For high partial waves, on the other hand, fission competes successfully with particle evaporation, and the ER cross sections drop below the fusion calculations. There is a only a restricted range (near the barrier) of cross sections $\simeq 100$ mb and of angular momenta $\simeq 25$–$30\hbar$, where the data agree with theory for both systems.

For lighter and/or more asymmetric systems simplified CC calculations work pretty well. As an example, we recall a recent study [34]) of fusion cross sections and $\langle l \rangle$ values in $^{28}Si + ^{154}Sm$; in that case simple CC calculations, analogous to those described in this work, are actually able to fit the dependence on energy of both $\langle l \rangle$ and fusion cross sections, from below to above the barrier.

An apparent counterexample of this trend is another recent work on $^{32}S + ^{100}Mo$

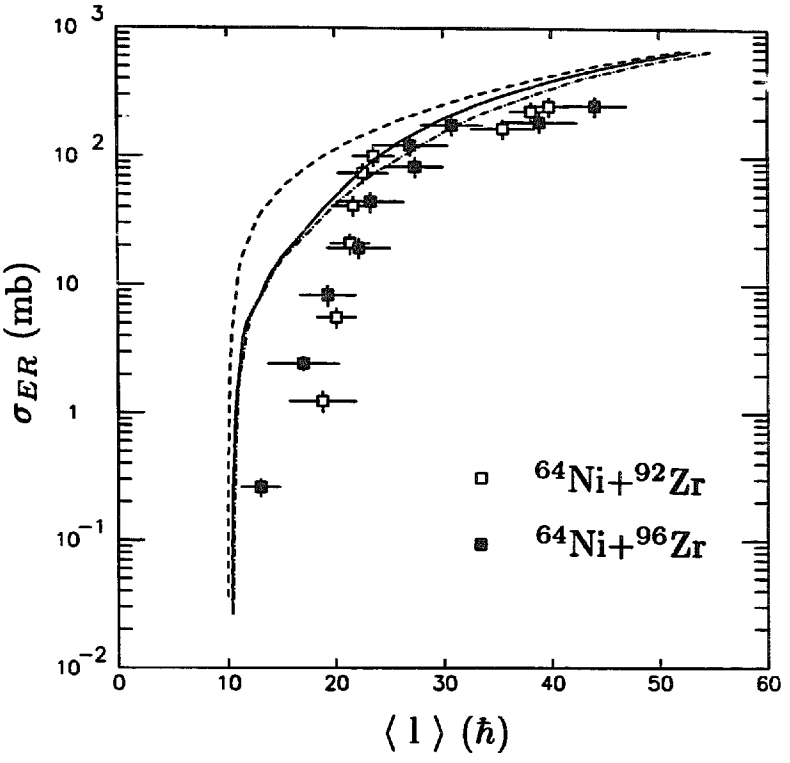

Fig. 6. ER cross sections versus $\langle l \rangle$ values for the two studied systems (see text).

and $^{36}S+^{96}Mo$ [ref. [35])]. The authors show that CCFUS calculations severely underpredict fusion cross sections and mean spin in the first system. But the existence in $^{32}S+^{100}Mo$ of very large and positive ($\simeq$6 MeV) Q-values for two-neutron pick-up and two-proton stripping, brings to the expectation of a strong influence of these channels on the fusion process, although no experimental results on transfer exist. In $^{36}S+^{96}Mo$, in fact, no positive Q-values for transfer are available, and the observation [35]) is that the corresponding CC calculations give an overall fair description of both fusion cross sections and $\langle l \rangle$.

The available data have been reviewed by Di Gregorio and Stokstad [3]) for all those cases where $\langle l \rangle$ and fusion cross sections were measured. They show that the standard CC model underpredicts both quantities below and at the barrier for heavy (quasi-)symmetric systems only. Adding our new data on $^{64}Ni+^{92,96}Zr$ to the systematics strengthens that observation.

The question is whether some approximations inherent to the CC theory simply break down for heavy symmetric systems. First, heavy nuclei often possess more low-lying collective states which are strongly coupled to the entrance channel and to other states. In other words, many degrees of freedom are available to the system, and the enhanced degree of complexity of the collisions is independently shown by recent observations of deep inelastic processes with significant cross sections for Ni+Sn [ref. [36])] and Ni+Zr [ref. [37])] already at sub-barrier energies.

Second, but not independently, higher-order coupling effects cannot be neglected even restricting the coupling scheme to a few low-lying inelastic excitations;

Esbensen and Landowne [38]) dedicated a paper to this problem. Summarizing the discussion of those authors, surface vibrational degrees of freedom are treated usually, as well as in the calculations presented in the present work, as independent harmonic oscillators *linearly* coupled to the relative motion through the deformation length parameter βR. Consequently, the elements of the nuclear interaction matrix are written in terms of the optical potential, its derivatives and powers of βR. For instance, to first order, the one-phonon excitation matrix element has the usual form

$$V_{01} = -\frac{\beta R}{(4\pi)^{1/2}} \frac{dU(r)}{dr}. \tag{4}$$

By allowing for second-order couplings, and for two-phonon excitations, one obtains matrix elements with terms in $(\beta R)^2$, whose effect on the low-energy fusion of heavy symmetric systems is predicted to be very significant. In ref. [38]) an application to the case of $^{58}Ni + ^{58}Ni$ is done, where it is shown that the calculated asymptotic barrier shift due to the linear + quadratic couplings is twice as large as the effect of the linear couplings only. Later, that model was successfully applied to the analysis of the elastic scattering [39]) of $^{58}Ni + ^{64}Ni$, where a good fit of the data, as well as of the fusion cross sections, was obtained with the full couplings. The strength of the interactions in the barrier region, which are weaker for light mass systems and/or for very asymmetric reactions, is an important parameter determining in which cases second- and possibly higher-order effects are not negligible. Also important is of course the excitation energy of the surface vibration. Detailed calculations would be welcome for the $^{64}Ni + ^{92,96}Zr$ systems.

5. Conclusions

In summary, we have presented the results of recent measurements of evaporation residue cross sections and mean angular momenta leading to fusion in the two systems $^{64}Ni + ^{92,96}Zr$, in an energy range encompassing the Coulomb barrier. The experiments have been carried out using the Legnaro recoil mass spectrometer and a more compact set-up employing an electrostatic field to deflect out the beam and beam-like particles at forward angles. The resulting ER cross sections agree with previously published data for $^{64}Ni + ^{96}Zr$, whereas large discrepancies show up with earlier measurements in $^{64}Ni + ^{92}Zr$. As for the ER $\langle l \rangle$ values, they exhibit the characteristic bump around the barrier and flatten out at higher energies due to the increasing competition from fission, in analogy with the evidences from the ER excitation functions. Both the barrier bump and the sub-barrier fusion enhancements cannot be reproduced by simple CC calculations, with an empirical ion-ion potential, and where the lowest-lying inelastic quadrupole and octupole excitations were considered. The additional effect of quasi-elastic transfer channels is predicted to be small.

These features are similar to what has been observed in $^{64}Ni + ^{100}Mo$, in contrast to a general systematics for lighter and/or more asymmetric systems where it seems

that even simplified CC calculations are able to treat and include the relevant degrees of freedom correctly, apart from particular cases where strongly coupled channels (e.g. positive Q-value transfer channels) need specific consideration. It has been pointed out that higher-order coupling effects should be taken into account in the calculation scheme [38]) for complex systems, as demonstrated by the success obtained by such a more complete CC model in the fit of the elastic scattering, fusion and transfer cross sections of $^{58}Ni + ^{64}Ni$ [refs. [39,40])]. Results of spin distribution measurements in the Ni + Ni systems have only preliminarly been reported some years ago [41]), but they would be quite important, by imposing more stringent tests to the model. At least equally welcome would be the results of explicit calculations for the Ni + Zr systems which have been the objects of the experimental investigations reported in this paper.

We like to thank F. Scarlassara and F. Soramel for participating in part of the experiments, the staff of the XTU Tandem Laboratory for their professional assistance, and A. Dal Bello for his skilful and invaluable technical help. A particular acknowledgment goes to G. Maron and G. Vedovato, for providing us with the hardware and the software for the data acquisition, and to Mr. G. Manente for high-quality target preparations.

References

1) Proc. Workshop on the interface between nuclear structure and heavy-ion reaction dynamics, Notre Dame, USA, 1990, ed. R.R. Betts and J.J. Kolata (IOP, Bristol, 1991)
2) Proc. Workshop on heavy-ion collisions near the Coulomb barrier, Daresbury, UK, 1990, ed. M.A. Nagarajan (IOP, Bristol, 1991)
3) D.E. Di Gregorio and R.G. Stokstad, Phys. Rev. **C43** (1991) 265
4) W. Kuehn, A. Ruckelshausen, R.D. Fischer, G. Breitbach, H.J. Hennrich, V. Metag, R. Novotny, R.V.F. Janssens, T.L. Khoo, D. Habs, D. Schwalm, B. Haas and R.S. Simon, Phys. Rev. Lett. **62** (1989) 1103
5) R.V.F. Janssens, R. Holzmann, W. Henning, T.L. Khoo, K.T. Lesko, G.S.F. Stephans, D.C. Radford, A.M. Van den Berg, W. Kuehn and R.M. Ronningen, Phys. Lett. **B181** (1986) 16
6) B. Haas, G. Duchene, F.A. Beck, T. Byrski, C. Gehringer, J.C. Merdinger, A. Nourredine, V. Rauch, J.P. Vivien, J. Barrette, S. Tobbeche, E. Bozek, J. Styczen, J. Keinonen, J. Dudek and W. Nazarewicz, Phys. Rev. Lett. **54** (1985) 398
7) A.M. Stefanini, L. Corradi, H. Moreno, L. Mueller, D.R. Napoli, P. Spolaore, E. Adamides, S. Beghini, G.F. Segato, F. Soramel and C. Signorini, Phys. Lett. **B252** (1990) 43
8) S. Beghini, C. Signorini, S. Lunardi, M. Morando, G. Fortuna, A.M. Stefanini, W. Meczynski and R. Pengo, Nucl. Instr. Meth. **A239** (1985) 585
9) F.L.H. Wolfs, R.V.F. Janssens, R. Holzmann, T.L. Khoo, W.C. Ma and S.J. Sanders, Phys. Rev. **C39** (1989) 865
10) P. Spolaore, J.D. Larson, C. Signorini, S. Beghini, X.K. Zhu and H.Z. Si, Nucl. Instr. Meth. **A238** (1985) 381;
A. Guerrieri, G. Maron, D.R. Napoli, G. Prete, Nucl. Instr. Meth., to be published
11) S. Gil, R. Vandenbosch, A. Charlop, A. García, D.D. Leach, S.J. Luke and S. Kailas, Phys. Rev. **C43** (1991) 701
12) S.H. Sie, J.O. Newton and J.R. Leigh, Nucl. Phys. **A245** (1981) 279
13) A. Ruckelshausen, R.D. Fischer, W. Kuehn, V. Metag, R. Muehlhans, R. Novotny, T.L. Khoo, R.V.F. Janssens, H. Groeger, D. Habs, R. Repnow, D. Schwalm, G. Duchene, R.M. Freeman, B. Haas, F. Haas, S. Hlavac and R.S. Simon, Phys. Rev. Lett. **56** (1986) 2356

14) D.J.G. Love, P.J. Bishop, A. Kirwan, P.J. Nolan, D.J. Thornley, A.H. Nelson and P.J. Twin, Phys. Rev. Lett. **57** (1986) 551
15) A. Ruckelshausen, B. Haas, D. Habs, R.V.F. Janssens, T.L. Khoo, W. Kuehn, V. Metag, D. Schwalm and R.S. Simon, Phys. Rev. Lett. **58** (1987) 1584
16) S. Gil, R. Vandenbosch, A.J. Lazzarini, D.-K. Lock and A. Ray, Phys. Rev. **C31** (1985) 1752
17) P.J. Nolan, D.J.G. Love, A. Kirwan, D.J. Unwin, A.H. Nelson, P.J. Twin and J.D. Garrett, Phys. Rev. Lett. **54** (1985) 2211
18) R.D. Fischer, A. Ruckelshausen, G. Koch, W. Kuehn, V. Metag. R. Muehlhans, R. Novotny, H. Stroeher, H. Groeger, D. Habs, H.W. Heyng, R. Repnow, D. Schwalm, W. Reisdorf and R.S. Simon, Phys. Lett. **B171** (1986) 33
19) M.L. Halbert, J.R. Beene, D.C. Hensley, K. Honkanen, T.M. Semkow, V. Abenante, D.G. Sarantites and Z. Li, Phys. Rev. **C40** (1989) 2558
20) A.H. Wuosmaa, R.R. Betts, B.B. Back, M.P. Carpenter, H. Esbensen, P.B. Fernandez, B.G. Glagola, Th. Happ, R.V.F. Janssens, T.L. Khoo, E.F. Moore, F. Scarlassara and P.H. Benet, Phys. Lett. **B263** (1991) 23
21) M.A. Lee, Nucl. Data Sheets **50** (1987) 563;
R.G. Helmer, Nucl. data Sheets **52** (1987) 1;
M.A. Lee, Nucl. Data Sheets **60** (1990) 419;
L.K. Peker, Nucl. Data Sheets **58** (1989) 93;
B. Singh, J.A. Szuecs and M.W. Johns, Nucl. Data Sheets **55** (1988) 185, and references therein
22) A. Gavron, Phys. Rev. **C20** (1980) 230
23) A. Ruckelshausen, B. Haas, D. Habs, R.V.F. Janssens, T.L. Khoo, W. Kuehn, V. Metag, D. Schwalm and R.S. Simon, Phys. Rev. Lett. **58** (1987) 1584
24) C.H. Dasso and S. Landowne, Comp. Phys. Commun. **46** (1987) 187
25) P.M. Endt. At. Data Nucl. Data Tables **23** (1979) 547; **26** (1981) 47
26) R.A. Broglia and A. Winther, Heavy-ion reactions, Lecture Notes, vol. 1 (Benjamin, New York, 1981)
27) P.R. Christensen and A. Winther, Phys. Lett. **B65** (1976) 19
28) M.H. Macfarlane and S.C. Pieper, Argonne National Laboratory Report ANL-76-11 (Rev. 1) 1978;
M.J. Rhoades-Brown, M.H. Macfarlane and S.C. Pieper, Phys. Rev. **C21** (1980) 2417, 2436
29) S.-W. Hong, T. Udagawa and T. Tamura, Nucl. Phys. **A491** (1989) 492;
T. Udagawa, T. Tamura and B. T. Kim, Phys. Rev. **C39** (1989) 1840
30) K.E. Rehm, Proc. Int. Symp. on heavy-ion reaction dynamics in tandem energy region, Hitachi, Japan, 1988, ed Y. Sugiyama, A. Iwamoto and H. Ikezoe (Universal Academy Press, Tokyo, 1989) p. 95
31) A.M. Stefanini, Proc. IV Int. Conf. on nucleus nucleus collisions, Kanazawa, Japan, 10-14 June, 1991, ed. H. Toki, I. Tenihata and H, Kamitsubo, Nucl. Phys. **A538** (1992) 195c
32) C.H. Dasso and S. Landowne, Phys. Rev. **C32** (1985) 1094
33) D.E. Di Gregorio, K.T. Lesko, B.A. Harmon, E.B. Norman, J. Pouliot, B. Sur, Y. Chan and R.G. Stokstad, Phys. Rev. **C42** (1990) 2108
34) S. Gil, D. Abriola, D.E. Di Gregorio, M. Di Tada, M. Elgue, A. Etchegoyen, M.C. Etchegoyen, J. Fernandez Niello, A.M.J. Ferrero, A.O. Macchiavelli, A.J. Pacheco, J.E. Testoni, P. Silveira Gomes, V.R. Vanin, A. Charlop, A. Garcia, S. Kailas, S.J. Luke, E. Renshaw and R. Vandenbosch, Phys. Rev. Lett. **65** (1990) 3100
35) H.-J. Hennrich, G. Breitbach, W. Kuehn, V. Metag, R. Novotny, D. Habs and D. Schwalm, Phys. Lett. **B258** (1991) 275
36) F.L.H. Wolfs, Phys. Rev. **C36** (1987) 1379
37) F. Scarlassara, S. Beghini, F. Soramel, C. Signorini, L. Corradi, G. Montagnoli, D.R. Napoli, A.M. Stefanini and Z.C. Li, Z. Phys. **A338** (1991) 171
38) H. Esbensen and S. Landowne, Phys. Rev. **C35** (1987) 2090
39) A.M. Stefanini, J.C. Xu, L. Corradi, G. Montagnoli, H. Moreno, Y. Nagashima, L. Mueller, M. Narayanasamy, D.R. Napoli, P. Spolaore, S. Beghini, F. Scarlassara, G.F. Segato, F. Soramel, C. Signorini, H. Esbensen, S. Landowne and G. Pollarolo, Phys. Lett. **B240** (1990) 306
40) H. Esbensen and S. Landowne, Nucl. Phys. **A492** 473
41) R. Rohe, Ph.D. Thesis, MIT (1984) unpublished